Research Square

Preprints are preliminary reports that have not undergone peer review.
They should not be considered conclusive, used to inform clinical practice,
or referenced by the media as validated information.

Short-term meteorological conditions and laboratory-confirmed influenza A in children: a time-series study with adjustment for testing volume

Jun Liu[1]
Bengbu Medical College
Chenyang Dong[1]
Bengbu Medical College
Yiwu Cheng
147925433240163.com

Bozhou People's Hospital

Research Article

Keywords: children, influenza A, meteorological factors, convective available potential energy, testing volume, time stratification, conditional quasi-Poisson

Posted Date: November 3rd, 2026

DOI: https://doi.org/10.21203/rs.3.rs-11331404/v1

License: This work is licensed under a Creative Commons Attribution 4.0 International License.
Read Full License

Additional Declarations: No competing interests reported.

Abstract

Background Hospital testing databases are widely used to study environmental drivers of influenza, but case counts are confounded by testing volume. We aimed to describe the temporal distribution of influenza A positivity in children and to screen short-term meteorological and air pollution exposures. We also distinguished absolute positivity burden from the probability of a positive result among those tested.

Methods We enrolled children aged 15 years or younger who underwent multiplex respiratory pathogen testing between 10 November 2024 and 30 November 2025, and built a daily time series anchored to illness onset. A time-stratified conditional quasi-Poisson model, stratified by year, month and day of week, used log(daily influenza A tests) as an offset. Thirty-five meteorological exposures (lag 0–7 d) and four air pollutants (lag 0–2 d) were standardised per 1 SD, with Benjamini-Hochberg correction for multiple comparisons.

Results Among 1675 children, 306 were positive for influenza A (18.3%); positivity peaked in December (149/322, 46.3%) and no cases were detected between March and September. After global correction, low convective available potential energy (CAPE) showed the strongest signal (rate ratio 0.103 per 1 SD increase, 95% CI 0.049–0.218, $q < 0.001$); the maximum thunderstorm index and thunderstorm index also reached $q < 0.05$. CAPE was negatively associated with the number of positive cases, the positivity rate among those tested and in the offset model, but not with the total number of tests. Mean temperature was negatively associated with both positive cases and total tests, but not in the positivity-rate or offset models. CAPE was consistent across the full observation window, restriction to onset-to-sampling of 7 d or less, sampling-date substitution and case-crossover analysis.

Conclusions In this single-centre, single-year cohort, low atmospheric instability, particularly low CAPE, was consistently associated with increased influenza A positivity in children and could not be explained by testing volume alone. The association between mean temperature and the absolute number of positive cases weakened markedly after denominator adjustment. CAPE is more plausibly a proxy for the cold-season synoptic situation than a direct cause, and these exploratory findings require multi-year, multi-centre validation.

Background

Acute respiratory infection in children is one of the most common disease burdens in paediatric outpatient, emergency and inpatient care, and infants and preschool children are particularly susceptible to seasonal respiratory pathogen epidemics [1]. Influenza A virus spreads rapidly, shows pronounced seasonal clustering and causes intense short-term outbreaks; it can drive transmission within schools and households and substantially increases paediatric consultations, pathogen testing and hospital admissions during epidemic peaks. Previous studies indicate that the seasonality of respiratory viruses is not a purely pathogen-specific phenomenon but the combined result of viral stability, host

susceptibility, population contact behaviour and meteorological background [2–4]. Analysing influenza A activity in children through short-term environmental variation may therefore help to explain its temporal fluctuations. It may also inform the allocation of clinical testing resources and seasonal early warning.

After the COVID-19 pandemic, the epidemic rhythms of common respiratory pathogens in children changed markedly, with delayed seasons, altered intensity, pathogen alternation and shifts in age structure reported in many settings [5–9]. This limits the reliability of judging influenza peaks from conventional calendar months or a single low-temperature indicator. Multi-pathogen time-series studies link temperature, humidity, wind speed and other weather conditions to paediatric respiratory pathogen activity, with varying strength and lag [7–9]. The direction of effect nevertheless differs across regions, pathogens and statistical models. Experimental and mechanistic studies further indicate that lower temperature and lower humidity increase the environmental stability and transmission efficiency of influenza virus. Cold exposure may also impair local antiviral defence in the airway epithelium [10–13]. Such mechanistic evidence, however, cannot replace environmental epidemiological evaluation in clinical populations.

For hospital-based multiplex pathogen testing databases, environmental association analyses face an important methodological problem: the daily number of influenza A-positive cases is influenced both by true pathogen activity and by the daily testing volume. When respiratory symptoms increase in the cold season, consultations, indications for testing, clinicians' test-ordering behaviour and departmental capacity may all change in parallel. The absolute number of positive cases can therefore rise appreciably even if the probability of a positive result among tested children is unchanged. Using only the daily number of positive cases as the outcome risks interpreting seasonal fluctuation in testing volume as a change in individual infection risk. It is therefore necessary to examine the number of positive cases, the total number of tests and the positivity rate among those tested simultaneously. The daily number of tests should also enter count models as an offset, distinguishing clinical testing burden from the positivity rate per unit of testing.

Beyond mean temperature and humidity, atmospheric stability, cloud cover, radiation and thunderstorm indices reflect the short-term synoptic situation across several dimensions. Convective available potential energy (CAPE) characterises atmospheric convective instability and is closely related to temperature, water vapour, radiation and boundary-layer state, yet its association with influenza A activity in children has not been systematically studied. We used multiplex pathogen testing records from Bozhou People's Hospital between November 2024 and November 2025, matched to daily MERRA-2 meteorological and urban air pollution data. 35 meteorological indicators and four air pollutants were screened within a unified statistical framework, with global FDR control for multiple comparisons. We then applied several analyses to representative exposures: daily lag analysis, low-dimensional DLNM, testing-volume decomposition, time-stratified case-crossover validation and sensitivity analyses. These tested whether the environmental signal remained stable after adjustment for testing volume. They also provide a basis for short-term environmental monitoring of paediatric influenza A and for future multi-year research.

Methods

1.1 Study design and participants

This was a single-centre retrospective time-series study. We enrolled children aged 15 years or younger who attended the outpatient or inpatient services of Bozhou People's Hospital. The enrolment period was 10 November 2024 to 30 November 2025. All children had undergone multiplex respiratory pathogen testing for symptoms of acute respiratory infection. Children with incomplete clinical records, those with repeated submissions for the same infectious episode, and those with immunosuppression as prespecified in the original study protocol were excluded. For each infectious episode only the first test record was retained, and the clinically recorded date of illness onset was used as the primary date of attribution. The study was reviewed and approved by the Ethics Committee of Bozhou People's Hospital (approval no. 2026-96). Informed consent requirements for this retrospective study were handled in accordance with the ethics approval.

1.2 Pathogen testing and definition of the influenza A outcome

Throat swabs or bronchoalveolar lavage fluid were collected and tested for 18 common respiratory pathogens using a multiplex PCR platform. The testing workflow and specimen handling followed the original study protocol [14–17]. Influenza A virus was the prespecified core pathogen; all 1675 children had an interpretable influenza A test result. The primary outcome was the daily number of children positive for influenza A. We also constructed three further outcomes to address variation in the testing denominator. These were the daily total number of influenza A tests, the positivity rate among those tested, and a count model with log(daily total number of tests) as an offset.

1.3 Meteorological and air pollution data

Same-period meteorological data were obtained from NASA MERRA-2 reanalysis products via the National Meteorological Science Data Center. Daily series were extracted for a representative grid point in the study area (115.75 E, 34.00 N) [18–20]. Complete meteorological data were obtained for 395 consecutive calendar days. The 35 meteorological indicators covered air pressure, temperature, humidity, precipitation, wind field, cloud cover, radiation, runoff and atmospheric instability. Convective available potential energy (CAPE) was used to characterise convective instability, and the thunderstorm index and maximum thunderstorm index served as related indicators of atmospheric instability. Air pollution data were obtained from the National Urban Air Quality Real-time Publishing Platform and included PM2.5, PM10, NO2 and O3-8h [21].

1.4 Exposure windows and data preprocessing

The primary screening window for meteorological exposures was defined as the lag 0–7 d moving average, and that for air pollution exposures as the lag 0–2 d moving average. Continuous exposures were standardised per 1 SD; for markedly skewed variables such as CAPE, low cloud cover, precipitation

and runoff, a log1p transformation was applied before standardisation. The primary analysis used a robust window that retained complete lag information while reducing boundary effects (1 December 2024 to 23 November 2025). The full observation period (10 November 2024 to 30 November 2025) was used in sensitivity analyses. Highly correlated exposures were flagged when the absolute Spearman rho was 0.70 or greater, to avoid mechanically combining strongly collinear variables in the same model.

1.5 Statistical analysis

All analyses were performed in R 4.4.2. All tests were two-sided, and $P < 0.05$ or FDR $q < 0.05$ was considered statistically significant. We first described the monthly number of influenza A tests, the number of positive cases and the positivity rate, and calculated descriptive statistics and a Spearman correlation matrix for the main meteorological exposures. The primary screening used a time-stratified conditional quasi-Poisson model, with calendar year, month and day of week as stratification variables. This controlled for long-term trend, season and day-of-week structure. log(daily number of influenza A tests) was included as an offset, giving the positivity rate ratio per unit of testing. The 35 meteorological exposures and four air pollution exposures formed a family of 39 primary exposures, and the P values from all 39 primary screening tests were corrected using the Benjamini-Hochberg procedure for global FDR. Effect sizes are reported as the RR and 95% CI per 1 SD increase in exposure. On the basis of effect magnitude, FDR results, exposure representativeness and collinearity structure in the primary screening, six exposures were selected for in-depth analysis: CAPE, low cloud cover, minimum temperature, mean temperature, diurnal temperature range and PM10. The in-depth analyses comprised: (1) daily lag 0–7 d effects with within-pathogen FDR; (2) low-dimensional DLNM, specified primarily as a linear exposure dimension plus a natural cubic spline lag dimension, to reduce the risk of overfitting single-year data [22]; (3) four-outcome decomposition comparing the number of positive cases, the total number of tests, the positivity rate among those tested and the offset model; (4) conventional time-stratified conditional logistic case-crossover validation; and (5) sensitivity analyses using the full observation window, restriction to onset-to-sampling of 7 d or less, and substitution of the sampling date for the onset date. Diagnostic analyses using different degrees of freedom for the time spline were also performed. Non-linear exposure and lag DLNM terms were exploratory only; when tail estimates produced extreme confidence intervals or numerical instability, they were not used for primary inference.

Results

2.1 Participants and overview of influenza A detection

A total of 1675 children were enrolled: 995 boys (59.4%) and 680 girls (40.6%), with a median age of 3.0 years (IQR 1.0–6.0). Of these, 306 were positive for influenza A, giving an overall positivity of 18.3%; 1155 children were positive for at least one respiratory pathogen, and 464 had co-detection of two or more pathogens. The median onset-to-sampling interval was 1 d, and 89 children (5.3%) had an interval of more than 7 d. Table 1 summarises the characteristics of the enrolled children and the influenza A testing results.

Table 1
Characteristics of the enrolled children and influenza A testing

Characteristic	Value
Total children enrolled	1675
Male	995 (59.4%)
Female	680 (40.6%)
Age, years	Median 3.0 (IQR 1.0–6.0)
Influenza A positive	306 (18.3%)
Positive for at least one pathogen	1155 (69.0%)
Co-detection of two or more pathogens	464 (27.7% of all; 40.2% of pathogen-positive)
Onset-to-sampling interval	Median 1 d
Onset-to-sampling > 7 d	89 (5.3%)

2.2 Temporal distribution of influenza A

Influenza A positivity showed a highly concentrated cold-season distribution. Positivity was 30.4% (7/23) in November 2024, rose to 46.3% (149/322) in December, the highest value of the study period, and was 27.6% (56/203) in January 2025 and 9.9% (15/152) in February. No influenza A-positive cases were detected between March and September 2025; positivity was 1.5% (2/137) in October and rose again to 28.0% (77/275) in November. This pattern indicates that influenza A activity in a single-year dataset overlaps strongly with the seasonal background, and subsequent models therefore used time stratification and several sensitivity analyses to control for seasonal structure. The monthly distribution of influenza A positivity is shown in Fig. 1.

Note

The line shows the proportion of tested children who were positive for influenza A in each month.

2.3 Description of environmental exposures and correlation structure

Over the 395 d study period, mean temperature was 16.63 degrees C (SD 10.23), minimum temperature 12.24 degrees C (SD 10.70), relative humidity 61.77% (SD 18.97%) and 10 m wind speed 2.84 m/s (SD 0.96). The distribution of CAPE was highly right-skewed, with a median of 0.66 J/kg (Q1 0, Q3 41.61), a mean of 200.90 J/kg and a maximum of 3306.21 J/kg; the median low cloud cover was 0.02. Marked correlation structure was present among temperature, radiation, air pressure, atmospheric instability and pollutants (Fig. 2). The primary analysis therefore used unified screening, FDR correction and in-depth

analysis of representative exposures, rather than forcing highly correlated indicators into the same multi-exposure model. Table 2 summarises the descriptive statistics of the main environmental indicators.

Table 2
Descriptive statistics of the main environmental indicators

Indicator	Mean (SD)	Median (Q1-Q3)	Range
Mean temperature (°C)	16.63 (10.23)	16.80 (7.72–25.67)	-5.78 to 34.38
Minimum temperature (°C)	12.24 (10.70)	13.01 (3.12–21.56)	-8.86 to 30.75
Relative humidity (%)	61.77 (18.97)	60.99 (46.21–77.54)	19.14 to 99.30
10 m wind speed (m/s)	2.84 (0.96)	2.74 (2.13–3.42)	0.92 to 6.88
Low cloud cover (0–1)	0.151 (0.259)	0.02 (0-0.175)	0 to 1
CAPE (J/kg)	200.90 (494.84)	0.66 (0-41.61)	0 to 3306.21
Thunderstorm index (K)	33.62 (10.27)	35.41 (27.96–41.15)	-11.19 to 53.27
Maximum thunderstorm index (K)	38.67 (9.54)	40.55 (33.34–45.30)	-6.10 to 58.42

Note

Red indicates positive and blue negative correlation; the depth of colour corresponds to the absolute value of the correlation coefficient.

2.4 Global screening of environmental exposures

Within the main robust window, the conditional quasi-Poisson model included 327 effective observation days and 84 calendar time strata. After global BH-FDR correction of the 39 environmental exposures, only three reached $q < 0.05$, all of them indicators of atmospheric instability. CAPE showed the strongest association: after log1p transformation, each 1 SD increase corresponded to an RR of 0.103 (95% CI 0.049–0.218; $q < 0.001$) for the influenza A positivity rate per unit of testing. The RR was 0.798 (0.707-0.900; $q = 0.0047$) for the maximum thunderstorm index and 0.832 (0.735–0.942; $q = 0.0462$) for the thunderstorm index. The RR for low cloud cover was 0.777 (0.650–0.929), but its global FDR q was 0.0555, which did not reach the prespecified threshold. Mean temperature, minimum temperature and PM10 did not pass global FDR in the primary screening. Table 3 presents the primary screening results, and Fig. 3 shows the testing-volume-adjusted results for the 20 exposures with the largest effect sizes among the 39 main environmental exposures.

Table 3
Time-stratified conditional quasi-Poisson screening results for the main environmental exposures

Exposure	RR per 1 SD	95% CI	P value	FDR q
CAPE	0.103	0.049–0.218	< 0.001	< 0.001
Maximum thunderstorm index	0.798	0.707-0.900	< 0.001	0.0047
Thunderstorm index	0.832	0.735–0.942	0.0036	0.0462
Low cloud cover	0.777	0.650–0.929	0.0057	0.0555
Ultraviolet radiation	0.428	0.228–0.805	0.0084	0.0637
Precipitation	0.726	0.559–0.943	0.0163	0.0755
Mean temperature	0.734	0.497–1.083	0.119	0.2450
PM10	1.047	0.900-1.219	0.550	0.7746

Note

Points are RRs per 1 SD increase, horizontal lines are 95% CIs and the dashed line is RR = 1; global BH-FDR q values are labelled on the left.

2.5 Daily lag patterns of the core exposures

CAPE showed RR < 1 at all eight single-day lags from lag 0 to lag 7 d and remained statistically significant after within-pathogen FDR correction. The effect was particularly evident at lags 3–5 d and 7 d. Low cloud cover showed a relatively stable negative association at lags 5–6 d. Mean and minimum temperature showed negative point estimates on some individual lag days but were generally unstable after within-pathogen FDR. PM10 showed positive nominal associations at lag 0 and lag 7 d, but no sustained multi-day pattern. The lag heat map for the core exposures is shown in Fig. 4.

Note

Colour represents log(RR); purple indicates RR < 1 and red RR > 1.

2.6 Decomposition of testing volume: differences between the CAPE and temperature signals

Four-outcome decomposition showed that the negative association of CAPE could not be explained by changes in testing volume alone. Per 1 SD increase in CAPE, the RR for the absolute number of positive cases was 0.061 (0.024–0.154) and the OR for the positivity rate among those tested was 0.060 (0.023–0.159). With the daily number of tests as an offset the RR was 0.103 (0.049–0.218), whereas the RR for

the total number of tests was 0.891 (0.756–1.049). Low cloud cover showed a similar but weaker pattern.

Mean temperature behaved differently. Per 1 SD increase, the RR was 0.516 (0.340–0.783) for the absolute number of positive cases and 0.709 (0.538–0.935) for the total number of tests. The OR for the positivity rate among those tested was 0.600 (0.339–1.062), and the RR in the offset model was 0.734 (0.497–1.083). Neither reached statistical significance. Minimum temperature showed a similar denominator-dependent pattern. These results indicate that the conventional association between low temperature and an increased number of positive cases largely overlapped with the concurrent increase in cold-season testing volume. CAPE, by contrast, remained significantly associated after denominator adjustment. Table 4 presents this decomposition across the four outcomes, and Fig. 5 shows it graphically.

Table 4
Decomposition of the effects of the core exposures across four outcomes

Exposure	RR, positive cases	RR, total tests	OR, positivity among those tested	RR, offset model
CAPE	0.061 (0.024–0.154)	0.891 (0.756–1.049)	0.060 (0.023–0.159)	0.103 (0.049–0.218)
Low cloud cover	0.615 (0.514–0.735)	0.969 (0.883–1.063)	0.714 (0.563–0.905)	0.777 (0.650–0.929)
Minimum temperature	0.508 (0.355–0.725)	0.675 (0.517–0.881)	0.634 (0.383–1.047)	0.757 (0.537–1.067)
Mean temperature	0.516 (0.340–0.783)	0.709 (0.538–0.935)	0.600 (0.339–1.062)	0.734 (0.497–1.083)
Diurnal temperature range	1.344 (1.142–1.582)	1.134 (1.006–1.278)	1.138 (0.881–1.470)	1.090 (0.909–1.307)
PM10	1.113 (0.944–1.313)	0.940 (0.837–1.055)	1.077 (0.864–1.342)	1.047 (0.900-1.219)

Note

For each exposure, the number of positive cases, the total number of tests, the positivity rate among those tested, and the positivity rate with the total number of tests as an offset are compared. The dashed line indicates an effect value of 1. RRs and ORs from different models are used to compare direction and robustness and should not be regarded as numerically equivalent.

2.7 Low-dimensional DLNM and sensitivity analyses

To reduce the risk of overfitting single-year data, the in-depth analysis used a low-dimensional DLNM specified as a linear exposure dimension plus a natural cubic spline lag dimension. Without additional co-exposures, the cumulative lag 0–7 d RR for low CAPE (P10 = 0 J/kg) relative to the median of 0.93

J/kg was 3.382 (2.293–4.986; global P < 0.001), and 3.571 (2.425–5.259) after adjustment for PM10. The cumulative RR for low cloud cover at P90 relative to the median was 0.375 (0.203–0.693), and 0.346 (0.189–0.634) after adjustment for PM10. The cumulative RR for mean temperature at P10 (2.224 degrees C) relative to the median of 17.87 degrees C was 1.641 (0.854–3.151), and 1.750 (0.914–3.349) after adjustment for PM10; neither reached statistical significance.

CAPE was consistent across several sensitivity analyses. The RR was 0.103 (0.049–0.218) in the main robust window and 0.096 (0.045–0.205) in the full observation window; it was 0.124 (0.059–0.258) after restriction to onset-to-sampling of 7 d or less and 0.158 (0.081–0.306) when the sampling date replaced the onset date. Conventional time-stratified conditional logistic case-crossover analysis yielded OR 0.061 (0.015–0.249, P < 0.001), consistent in direction. Low cloud cover likewise maintained RR < 1 in the above sensitivity analyses. By contrast, mean temperature was not significant in the main robust window or after restriction to 7 d or less. It became significant only in the full observation window and in the sampling-date analysis, indicating weaker stability than CAPE. Table 5 summarises the main robustness analyses, and Table 6 presents the cumulative lag 0–7 d effects from the low-dimensional DLNM.

Table 5
Main robustness analyses for CAPE and low cloud cover

Analysis	**CAPE effect (95% CI)**	**Low cloud cover effect (95% CI)**
Main robust window (conditional quasi-Poisson)	RR 0.103 (0.049–0.218)	RR 0.777 (0.650–0.929)
Full observation window	RR 0.096 (0.045–0.205)	RR 0.693 (0.585–0.821)
Onset-to-sampling 7 d or less	RR 0.124 (0.059–0.258)	RR 0.759 (0.635–0.906)
Sampling date substituted for onset date	RR 0.158 (0.081–0.306)	RR 0.714 (0.610–0.834)
Conventional conditional logistic case-crossover	OR 0.061 (0.015–0.249)	OR 0.615 (0.469–0.806)

Table 6
Cumulative lag 0–7 d effects of the core exposures in the low-dimensional DLNM

Exposure contrast	Without PM10	Adjusted for PM10
CAPE P10 (0) vs median 0.93 J/kg	RR 3.382 (2.293–4.986)	RR 3.571 (2.425–5.259)
Low cloud cover P90 (0.52) vs median 0.02	RR 0.375 (0.203–0.693)	RR 0.346 (0.189–0.634)
Minimum temperature P10 (-3.414°C) vs median 13.4°C	RR 1.446 (0.822–2.543)	RR 1.562 (0.888–2.748)
Mean temperature P10 (2.224°C) vs median 17.87°C	RR 1.641 (0.854–3.151)	RR 1.750 (0.914–3.349)
PM10 P90 (126) vs median 58.50 μg/m³	RR 1.253 (0.966–1.624)	RR 1.242 (0.943–1.635)

2.8 Model stability and numerical diagnostics

Alternative time-trend models indicated that seasonal structure in the single-year data remained the main source of uncertainty. For CAPE, point estimates were RR < 1 with conventional model P < 0.05 at time spline df of 4, 6, 7 and 8, but the effect attenuated markedly at df 10–12. Some time-series diagnostics also indicated that residual autocorrelation persisted. The time-stratified conditional quasi-Poisson model was therefore retained as the primary inferential framework, and results from high-df time splines were regarded as a robustness boundary rather than as a replacement for the primary model.

Exploratory non-linear exposure and lag DLNM terms produced extreme effect estimates and very wide confidence intervals in the distribution tails of CAPE, temperature and other variables. A single-year sample therefore provides insufficient information for high-dimensional non-linear models. We accordingly do not present these tail non-linear curves as main figures and do not infer thresholds or U- or J-shaped relationships from them. Primary inference rests on the low-dimensional DLNM with prespecified degrees of freedom, on standardised linear effects, on denominator decomposition and on consistency across designs.

Discussion

In this study we extracted influenza A from the multiplex testing records of 1675 children and re-evaluated short-term environmental associations after explicitly adjusting for daily testing volume, yielding three main findings. First, influenza A was strongly concentrated in the cold season, with the main positivity peaks in December 2024, January 2025 and November 2025 and no positive cases detected between March and September 2025. Second, in the unified global screening of 39 environmental exposures, indicators of atmospheric instability proved more stable than conventional temperature indicators, with the strongest signal for CAPE. The thunderstorm index and maximum

thunderstorm index also passed FDR correction. Third, denominator decomposition showed that the negative association between mean temperature and the absolute number of positive cases was accompanied by a concurrent decline in testing volume. Once the testing denominator was taken into account, this association became non-significant. CAPE, in contrast, retained a strong negative association with the number of positive cases, with the positivity rate among those tested, and in the offset model. CAPE showed no clear association with the total number of tests.

These results indicate that, in clinical testing databases, the number of positive cases and the probability of a positive result must be strictly distinguished. Previous studies of meteorology and respiratory infection have often used daily case counts as the outcome, but daily case counts in hospital data are influenced by both consultation and testing behaviour. The proportion of laboratory tests that are positive is itself a biased indicator. It deviates systematically from the true incidence of infection as testing rates change, as other pathogens with similar symptoms circulate, and as healthcare-seeking behaviour differs between age groups. It therefore requires cautious interpretation and, where possible, adjustment using information on testing volume [23]. In respiratory virus surveillance, tested children are not a random sample of the population. Indications for testing, the timing of presentation and clinicians' test-ordering behaviour all systematically alter the infection probability of those tested. Evaluations based on the number of positive detections are therefore easily confounded by changes in the denominator. The test-negative design conditions on the shared behaviour of being tested and compares positive with negative individuals within the tested population. It can thereby reduce substantially the selection bias arising from differences in healthcare-seeking behaviour [24, 25]. Its underlying logic is the same as that of the offset model used here, namely restricting the comparison to a unit of testing. Our mean temperature result illustrates this difference. The apparent association between higher temperature and fewer positive cases was accompanied by a concurrent decline in the total number of tests. The association attenuated markedly once the outcome was changed to the positivity rate among those tested, or once a testing-volume offset was added to the count model. Absolute counts alone therefore cannot support the conclusion that low temperature increases the probability of influenza A infection in an individual.

The CAPE result differed from that for temperature. CAPE measures convective instability, and low values generally correspond to a more stable atmosphere. In this study, low CAPE was associated with a higher influenza A positivity rate and did not depend on an increase in testing volume. This was consistent with the same-direction FDR results for the maximum thunderstorm index and the thunderstorm index. CAPE may therefore mark the cold-season stable weather background in this region more effectively than conventional indicators. Synoptic-scale indicators have precedent in influenza research. Across 79 cities in the United States, the presence of cold-season polar air masses was associated with a significantly higher probability of influenza, whereas tropical air masses were associated with a markedly lower one [26]. Convective weather systems can also trigger clustered outbreaks of respiratory disease within hours. During the 2016 Melbourne epidemic thunderstorm asthma event, respiratory emergency and intensive care presentations rose sharply [27]. Downdraft

convective available potential energy (DCAPE), which belongs to the same family as convective instability, reached high to very high thresholds before the event [28]. This evidence, however, comes from acute respiratory events such as thunderstorm asthma and is triggered by high instability. That is opposite in direction to the association observed here between low instability and increased positivity. No study has yet used CAPE as the exposure with influenza positivity as the outcome. CAPE is therefore more likely to be an efficient proxy for the overall winter synoptic situation than a direct cause.

The sensitivity of influenza virus to temperature and humidity has a substantial experimental basis. Low temperature and lower absolute humidity favour the stability and transmission of influenza virus, and low temperature may also impair local antiviral defence in the airway [10–13]. The present study does not contradict these mechanisms. It suggests, however, that in these single-centre clinical testing data the independent statistical signal of mean temperature for overall influenza A positivity is less stable than that of CAPE. One possible reason is that temperature is almost completely collinear with season, whereas CAPE and related instability indicators may integrate information on temperature, water vapour and convective background. Another factor that cannot be ignored is behavioural confounding: influenza A transmission in children depends heavily on school clustering and household contact. An ecological study of school-age children in Guangzhou, China, using data from 2010 to 2023 showed that influenza transmission declined markedly during school holidays. Transmission peaked in the third to fourth week after children returned to school. This suggests that changes in population contact structure caused by term schedules and holidays may themselves explain a substantial part of epidemic fluctuation [29]. Within a single seasonal cycle, such changes in contact structure are closely synchronised in time with the cold season and are difficult to separate fully from meteorological effects. The temperature result should therefore be understood as failing to remain stable under testing-volume adjustment and seasonal stratification, rather than as a refutation of temperature and humidity mechanisms. These explanations still require validation with multi-year data, and mechanisms cannot be determined from the present results alone.

We also observed a stable negative signal for low cloud cover. Its global FDR q in the primary screening was 0.0555, slightly above 0.05. The direction was nevertheless consistent across four-outcome decomposition, the full observation window, restriction to 7 d or less and sampling-date substitution. It was also confirmed in the conventional conditional logistic model. Low cloud cover may therefore be regarded as a secondary exploratory signal and should not be placed alongside CAPE as a main conclusion. PM10 behaved differently. Its results were inconsistent across analysis windows, with no clear association in either the main robust window or the denominator-adjusted models. Air pollution is therefore not supported as a main explanatory factor in this paper. It should be noted that this negative finding is not entirely consistent with previous evidence. A multi-city time-series study based on five years of surveillance data from 82 Chinese cities examined this question. Apart from ozone, higher daily concentrations of most air pollutants were positively associated with reported influenza incidence in the short term [30]. The pollutants examined included PM2.5, PM10, NO2 and SO2, and NO2 remained significant after simultaneous adjustment for all six pollutants. The unstable PM10 result may relate to

coverage of a single city, limited temporal variation in pollutant concentrations, strong collinearity between particulate matter and temperature, and the choice of exposure window. It may also reflect regional differences in pollutant composition and influenza surveillance.

This study has several methodological strengths. First, rather than analysing a single temperature indicator, we placed 35 meteorological variables and four air pollutants in a unified screening family and applied global FDR correction. This reduced the risk of post hoc selection of the smallest P value. Second, the daily number of tests was included as an offset in the primary model, and the number of positive cases, the total number of tests and the positivity rate were compared in parallel. This allowed testing-volume-driven artefacts to be identified. Third, the primary results used a time-stratified conditional quasi-Poisson framework and were cross-validated by conventional conditional logistic case-crossover, the full time window, substitution of the sampling date and restriction to 7 d or less. Fourth, numerical instability in high-dimensional non-linear models was not over-interpreted, and primary inference was restricted to the low-dimensional DLNM and to reproducible directions of effect.

The limitations are equally clear. First, this was a single-centre study with an observation period of about 13 months, covering only one complete seasonal cycle. Between-year variation therefore cannot be estimated stably, and any meteorological indicator strongly collinear with winter may be subject to residual seasonal confounding. Second, influenza A was continuously zero between March and September 2025, indicating a highly seasonally concentrated outcome that can produce separation or extreme estimates in some high-dimensional models. The large effect size for CAPE should therefore be judged mainly on direction and consistency across models, rather than used for precise causal quantification. Third, although the time-stratified design controls for month and day-of-week structure, alternative time-spline diagnostics still indicated residual autocorrelation, suggesting that unmeasured seasonal factors may persist. Fourth, meteorological data came from a representative regional grid and pollution data from fixed urban monitoring stations, neither of which represents individual exposure. Fifth, potential influencing factors such as indications for testing, antiviral treatment, influenza vaccination, school exposure, household clustering and viral subtype could not be included. At least three to five complete years of multi-centre data, with prespecified hypotheses regarding CAPE and atmospheric stability, are needed for external validation.

Conclusions

In single-centre paediatric respiratory testing data from November 2024 to November 2025, influenza A positivity was highly concentrated in the cold season. After adjustment for daily testing volume as an offset, and after global FDR control across 39 environmental exposures, indicators of low atmospheric instability were consistently associated with a higher influenza A positivity rate. This was most evident for low CAPE. The signal was consistent in direction across daily lags, the full observation window, sampling-date substitution, restriction to 7 d or less and conventional case-crossover analysis. By contrast, the association between mean temperature and the absolute number of positive cases attenuated markedly after adjustment for the testing denominator. At this stage, CAPE and related

instability indicators are better interpreted as markers of the overall weather background of cold-season influenza A activity in this region than as direct causal risk factors. Given the single-year, single-centre design and strong seasonal collinearity, this study should be positioned as exploratory and hypothesis-generating, requiring further validation with multi-year, multi-centre data.

Abbreviations

CAPE
convective available potential energy
CI
confidence interval
DCAPE
downdraft convective available potential energy
DLNM
distributed lag non-linear model
FDR
false discovery rate
IQR
interquartile range
MERRA-2
Modern-Era Retrospective analysis for Research and Applications, version 2
NO2
nitrogen dioxide
O3-8h
maximum 8-hour average ozone
OR
odds ratio
PCR
polymerase chain reaction
PM2.5
particulate matter with an aerodynamic diameter of 2.5 μm or less
PM10
particulate matter with an aerodynamic diameter of 10 μm or less
RR
rate ratio
SD
standard deviation
SO2
sulfur dioxide.

Declarations

Ethics approval and consent to participate

This study was reviewed and approved by the Ethics Committee of Bozhou People's Hospital (approval no. 2026-96). Informed consent requirements for this retrospective study were handled in accordance with the ethics approval.

Availability of data and materials

The datasets generated and analysed during the current study are not publicly available owing to patient confidentiality but are available from the corresponding author on reasonable request.

Competing interests

The authors declare that they have no competing interests.

Funding

This research received no specific grant from any funding agency in the public, commercial or not-for-profit sectors.

Authors' contributions

JL and CD designed the study, collected and analysed the data, and drafted the manuscript. YC conceived and supervised the study, interpreted the data, and critically revised the manuscript. All authors read and approved the final manuscript.

Use of large language models

Large language model tools were used to assist with language editing, translation and structural revision of the manuscript and to identify candidate references, which were independently verified by the authors. All scientific content, data analysis, interpretation and conclusions were produced and verified by the authors, who take full responsibility for the work.

References

1. GBD 2019 LRI Collaborators. Age-sex differences in the global burden of lower respiratory infections and risk factors, 1990–2019: results from the Global Burden of Disease Study 2019. Lancet Infect Dis. 2022;22(11):1626–47. 10.1016/S1473-3099(22)00510-2.
2. Moriyama M, Hugentobler WJ, Iwasaki A. Seasonality of respiratory viral infections. Annu Rev Virol. 2020;7(1):83–101. 10.1146/annurev-virology-012420-022445.
3. Pica N, Bouvier NM. Environmental factors affecting the transmission of respiratory viruses. Curr Opin Virol. 2012;2(1):90–5. 10.1016/j.coviro.2011.12.003.

4. Shang X, Zheng J, Liu X, et al. Climatic factors drive global viral respiratory infections with regional heterogeneity: a systematic review and meta-analysis. Environ Int. 2026;208:110120. 10.1016/j.envint.2026.110120.
5. Liu P, Xu M, Lu L, et al. Resurgence of common respiratory viruses and Mycoplasma pneumoniae after ending the zero-COVID policy in Shanghai. Sci Rep. 2025;15(1):1765. 10.1038/s41598-025-85852-z.
6. Li H, Yang Y, Tao R, Shang S. Analyzing infections caused by 11 respiratory pathogens in children: pre- and post-COVID-19 pandemic trends in China. J Med Virol. 2024;96(9):e29929. 10.1002/jmv.29929.
7. Li C, Xi L, Rao J, Tang F, Xiang Y, Wang X. Epidemiological trends and climatic drivers of pediatric respiratory infections in Wuhan, China: a multi-pathogen analysis. Front Cell Infect Microbiol. 2025;15:1624638. 10.3389/fcimb.2025.1624638.
8. Wang B, Zhang H, Liang S, et al. Epidemiological trends and climate-driven dynamics of children respiratory infections in Lanzhou, China: a multi-pathogen time-series analysis. Front Cell Infect Microbiol. 2026;16:1777468. 10.3389/fcimb.2026.1777468.
9. Luo C, Wang X, Zhou N. Epidemiological characteristics of pediatric respiratory pathogens and their association with climate in Wuxi, Chongqing, China. New Microbes New Infect. 2025;68:101656. 10.1016/j.nmni.2025.101656.
10. Shaman J, Kohn M. Absolute humidity modulates influenza survival, transmission, and seasonality. Proc Natl Acad Sci U S A. 2009;106(9):3243–8. 10.1073/pnas.0806852106.
11. Lowen AC, Mubareka S, Steel J, Palese P. Influenza virus transmission is dependent on relative humidity and temperature. PLoS Pathog. 2007;3(10):e151. 10.1371/journal.ppat.0030151.
12. Foxman EF, Storer JA, Fitzgerald ME, et al. Temperature-dependent innate defense against the common cold virus limits viral replication at warm temperature in mouse airway cells. Proc Natl Acad Sci U S A. 2015;112(3):827–32. 10.1073/pnas.1411030112.
13. Huang D, Taha MS, Nocera AL, Workman AD, Amiji MM, Bleier BS. Cold exposure impairs extracellular vesicle swarm-mediated nasal antiviral immunity. J Allergy Clin Immunol. 2023;151(2):509–e5258. 10.1016/j.jaci.2022.09.037.
14. Bradley JS, Byington CL, Shah SS, et al. The management of community-acquired pneumonia in infants and children older than 3 months of age: clinical practice guidelines by the Pediatric Infectious Diseases Society and the Infectious Diseases Society of America. Clin Infect Dis. 2011;53(7):e25–76. 10.1093/cid/cir531.
15. World Health Organization. Revised WHO classification and treatment of childhood pneumonia at health facilities: evidence summaries. Geneva: World Health Organization; 2014.
16. Krause JC, Panning M, Hengel H, Henneke P. The role of multiplex PCR in respiratory tract infections in children. Dtsch Arztebl Int. 2014;111(38):639–45. 10.3238/arztebl.2014.0639.
17. Esposito S, Mencacci A, Cenci E, Camilloni B, Silvestri E, Principi N. Multiplex platforms for the identification of respiratory pathogens: are they useful in pediatric clinical practice? Front Cell Infect

Microbiol. 2019;9:196. 10.3389/fcimb.2019.00196.

18. Gelaro R, McCarty W, Suarez MJ, et al. The Modern-Era Retrospective Analysis for Research and Applications, Version 2 (MERRA-2). J Clim. 2017;30(14):5419–54. 10.1175/JCLI-D-16-0758.1.
19. Global Modeling and Assimilation Office. MERRA-2 inst3_3d_asm_Nv: 3d, 3-Hourly, Instantaneous, Model-Level, Assimilation, Assimilated Meteorological Fields V5.12.4 (M2I3NVASM) [dataset]. NASA Goddard Earth Sciences Data and Information Services Center. 10.5067/WWQSXQ8IVFW8
20. Global Modeling and Assimilation Office. MERRA-2 statD_2d_slv_Nx: 2d, Daily, Aggregated Statistics, Single-Level, Assimilation, Single-Level Diagnostics V5.12.4 (M2SDNXSLV) [dataset]. NASA Goddard Earth Sciences Data and Information Services Center. 10.5067/9SC1VNTWGWV3
21. China National Environmental Monitoring Centre. National Urban Air Quality Real-time Publishing Platform. Available at: https://air.cnemc.cn:18007/. Accessed September 17, 2026.
22. Gasparrini A, Armstrong B, Kenward MG. Distributed lag non-linear models. Stat Med. 2010;29(21):2224–34. 10.1002/sim.3940.
23. Eales O, McCaw JM, Shearer FM. Biases in routine influenza surveillance indicators used to monitor infection incidence and recommendations for improvement. Influenza Other Respir Viruses. 2024;18(12):e70050. 10.1111/irv.70050.
24. Jackson ML, Nelson JC. The test-negative design for estimating influenza vaccine effectiveness. Vaccine. 2013;31(17):2165–8. 10.1016/j.vaccine.2013.02.053.
25. Sullivan SG, Tchetgen Tchetgen EJ, Cowling BJ. Theoretical basis of the test-negative study design for assessment of influenza vaccine effectiveness. Am J Epidemiol. 2016;184(5):345–53. 10.1093/aje/kww064.
26. Zhao N, Cao G, Vanos JK, Vecellio DJ. The effects of synoptic weather on influenza infection incidences: a retrospective study utilizing digital disease surveillance. Int J Biometeorol. 2018;62(1):69–84. 10.1007/s00484-017-1306-4.
27. Thien F, Beggs PJ, Csutoros D, et al. The Melbourne epidemic thunderstorm asthma event 2016: an investigation of environmental triggers, effect on health services, and patient risk factors. Lancet Planet Health. 2018;2(6):e255–63. 10.1016/S2542-5196(18)30120-7.
28. Grundstein A, Shepherd M, Miller P, Sarnat SE. The role of mesoscale-convective processes in explaining the 21 November 2016 epidemic thunderstorm asthma event in Melbourne, Australia. J Appl Meteorol Climatol. 2017;56(5):1337–43. 10.1175/JAMC-D-17-0027.1.
29. Liu Y, Chen Z, Zhang M, et al. Vacation and back-to-school effect on influenza transmission among school-age children in Guangzhou, China: an ecological study from 2010 to 2023. BMJ Open. 2025;15(6):e096341. 10.1136/bmjopen-2024-096341.
30. Yu LJ, Li XL, Wang YH, et al. Short-term exposure to ambient air pollution and influenza: a multicity study in China. Environ Health Perspect. 2023;131(12):127010. 10.1289/EHP12146.

Figures

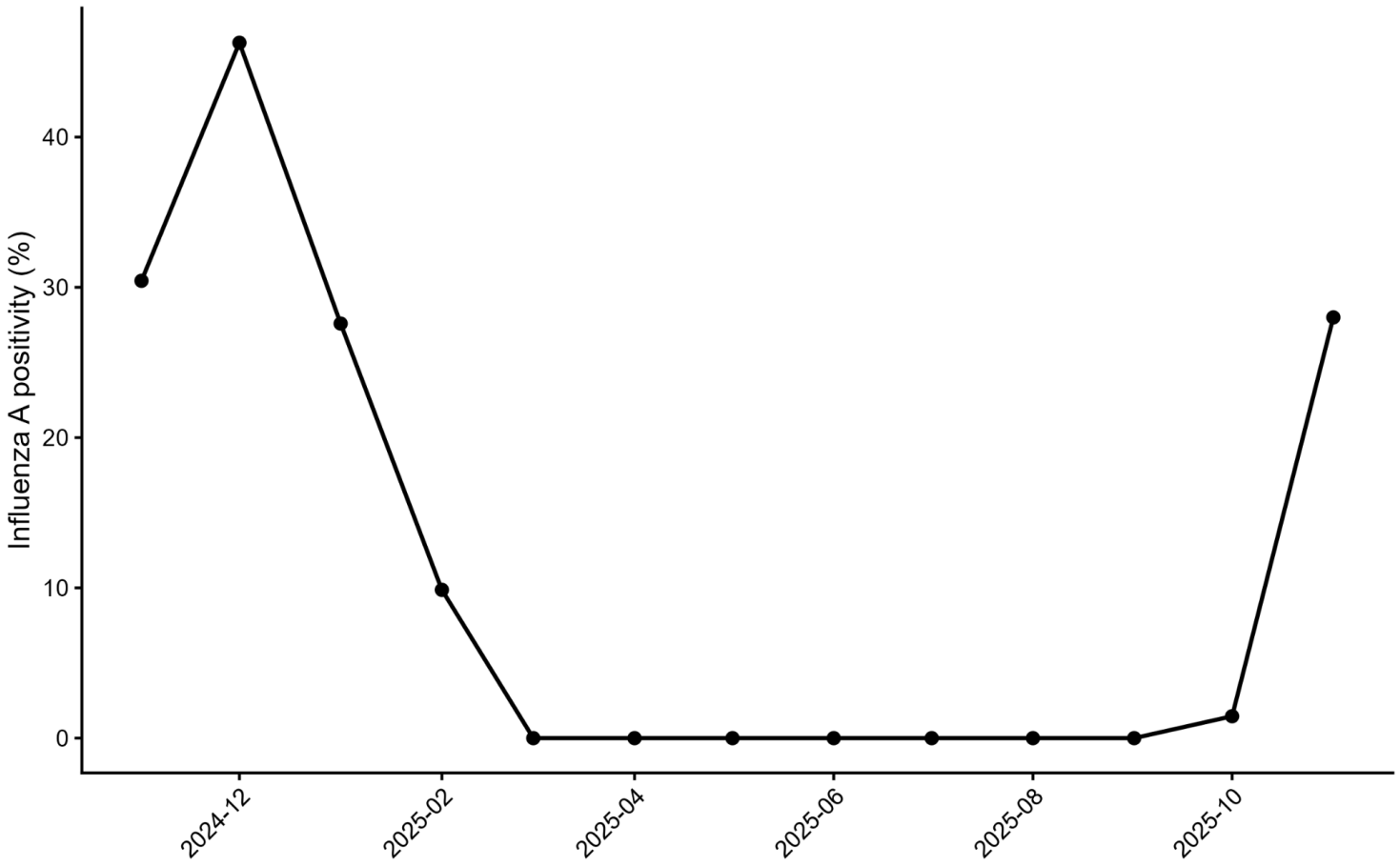


Figure 1

Monthly influenza A positivity among children, November 2024 to November 2025

Note: The line shows the proportion of tested children who were positive for influenza A in each month.

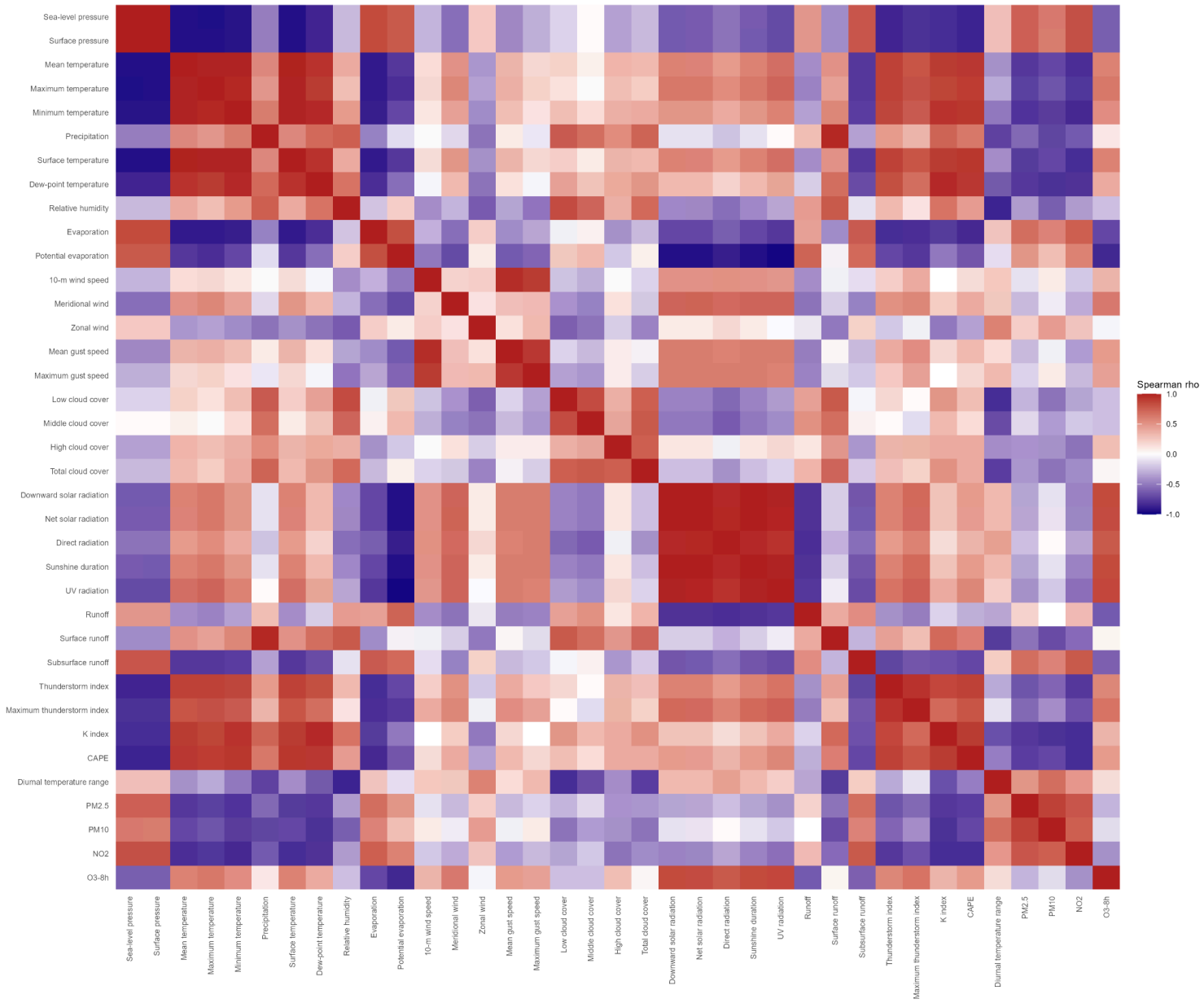


Figure 2

Spearman correlation matrix of the main meteorological factors and air pollutants

Note: Red indicates positive and blue negative correlation; the depth of colour corresponds to the absolute value of the correlation coefficient.

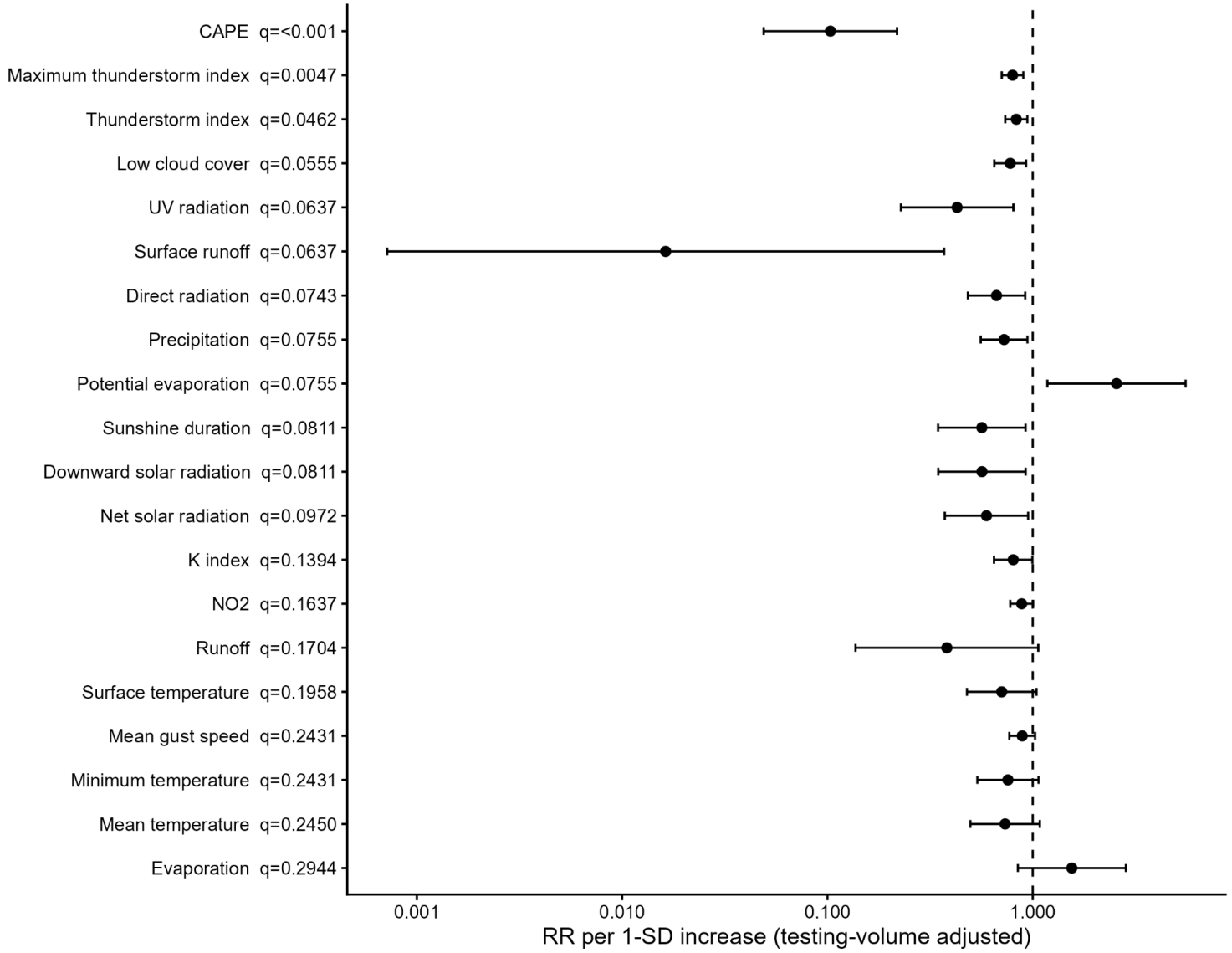


Figure 3

Testing-volume-adjusted effects of the 20 strongest exposures

Note: Points are RRs per 1 SD increase, horizontal lines are 95% CIs and the dashed line is RR=1; global BH-FDR q values are labelled on the left.

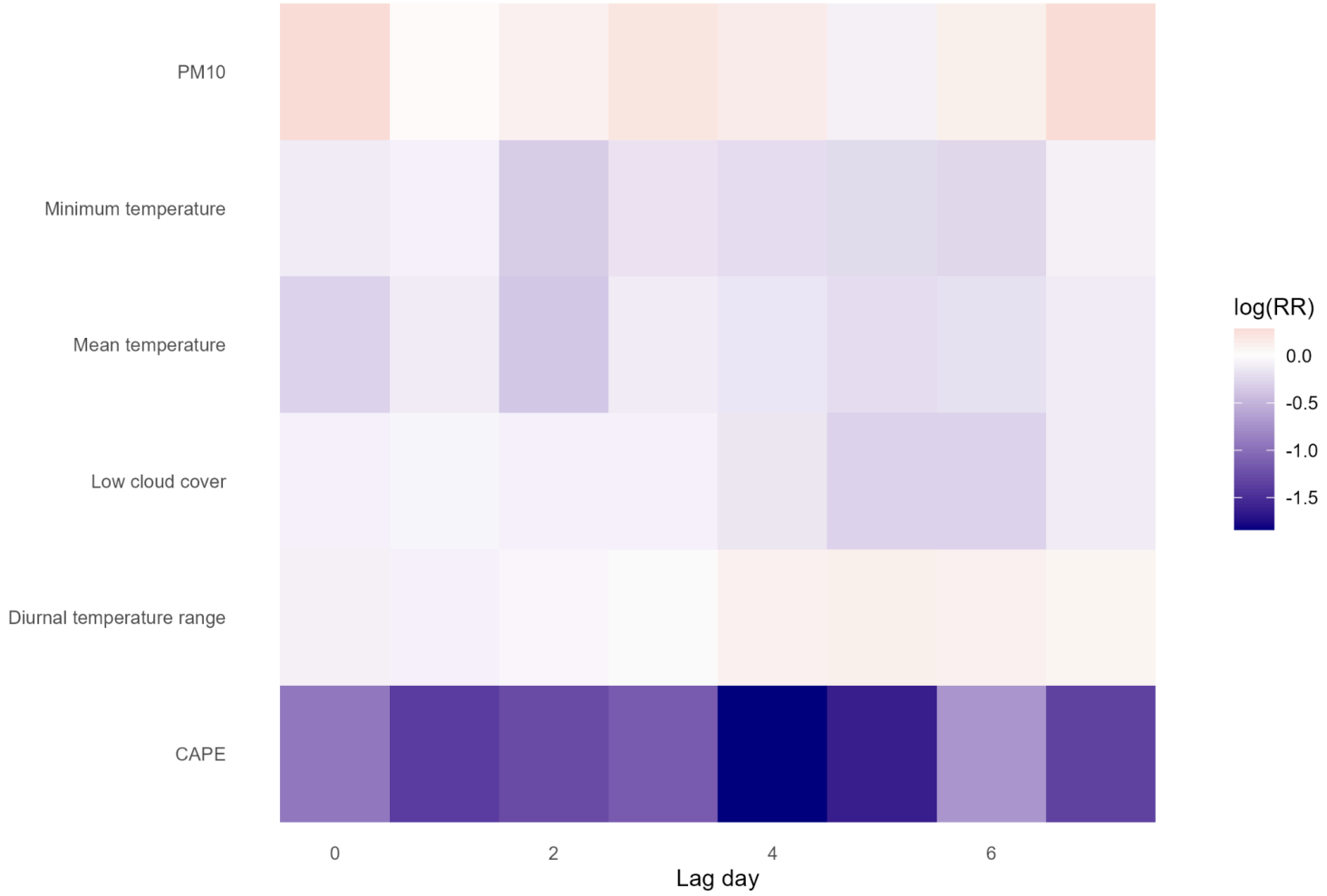


Figure 4

Heat map of lag 0-7 d effects for the core environmental exposures

Note: Colour represents log(RR); purple indicates RR<1 and red RR>1.

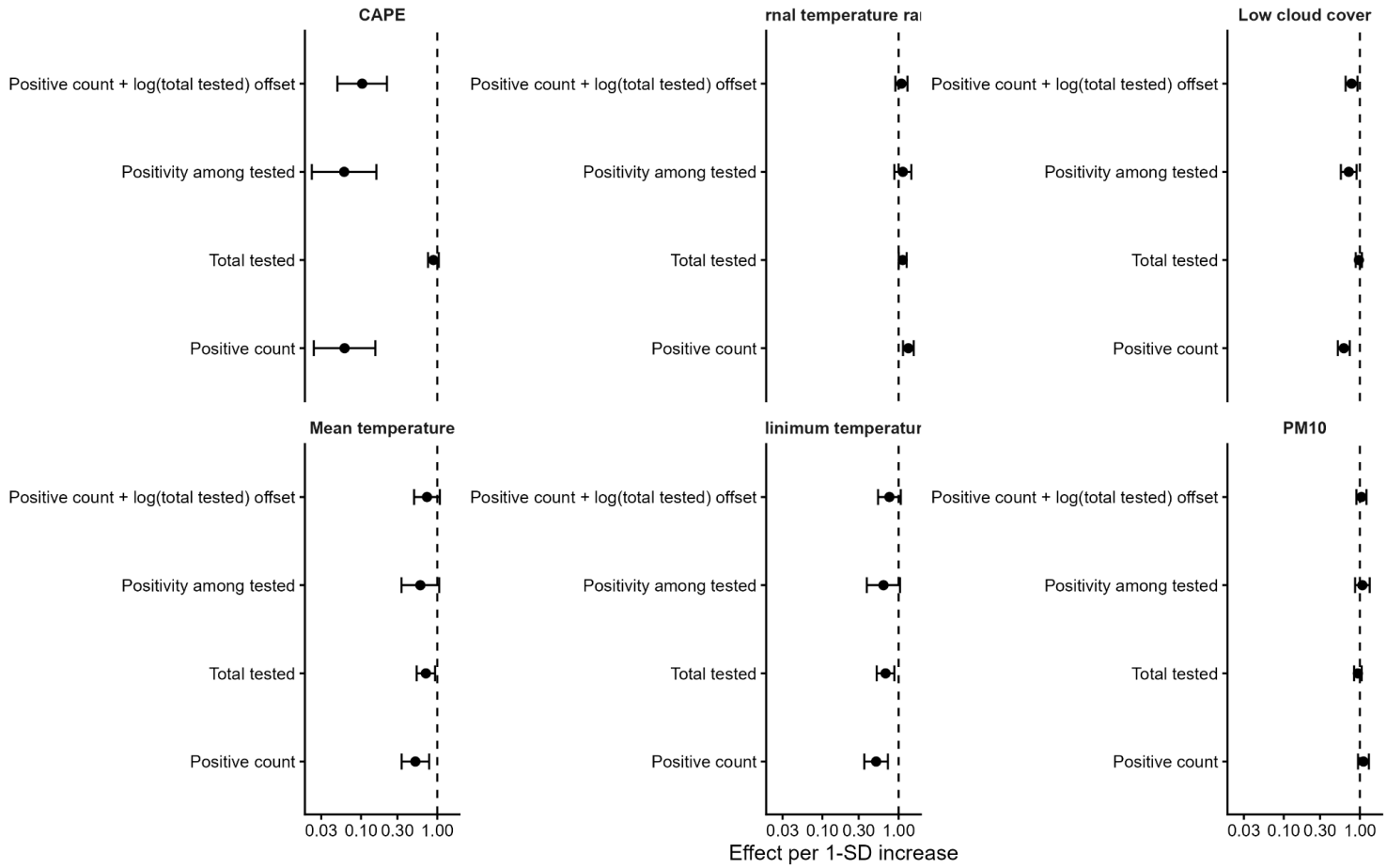


Figure 5

Testing-volume decomposition of the core exposures

Note: For each exposure, the number of positive cases, the total number of tests, the positivity rate among those tested, and the positivity rate with the total number of tests as an offset are compared. The dashed line indicates an effect value of 1. RRs and ORs from different models are used to compare direction and robustness and should not be regarded as numerically equivalent.